Flow Separation Patterns over an F-14A Aircraft Wing

Tsze C. Tai*
David Taylor Research Center, Bethesda, Maryland 20084

Computational results of flow over an F-14A wing based on a thin-layer Navier-Stokes method are presented, and the resulting flow separation patterns are discussed. A zonal approach is employed that allows a condensed grid for viscous calculations near the wing surface. The F-14A wing is fixed with a sweep angle of 20 deg and travels at an altitude of 45,000 ft above sea level at Mach 0.6 and at sea level at Mach 0.1 with various angles of attack. These conditions, which yield a Reynolds number of 8.95×10^6 at both altitudes, allow evaluation of the effect of Mach number on flow separation patterns with fixed Reynolds number. Massive flow separation occurs at Mach 0.6 at an angle of attack of 10 deg. At Mach 0.1, with the same Reynolds number, the rear region massive separation disappears, but a strong leading-edge separation emerges. Consequently, the lift and drag values are far more stable at low speed as the angle of attack increases.

Introduction

THE criterion for flow separation in three dimensions is radically different from that of the conventional concept based on two-dimensional flow. In three-dimensional flow, the concept of the envelope of limiting streamlines as the separation line has been used. First suggested by Eichelbrenner and Oudart,[1] the envelope concept was further explored by Maskell[2] through general flow observations and supported by Wang[3] from the standpoint of numerical results. Two basic forms of separation patterns in three dimensions have been observed: the bubble type and the vortex-layer type, sometimes referred to as closed separation and open separation, respectively. For most flows of practical interest, the separation is of the vortex-layer type, where vortices are created as a result of the convergence of viscous streamlines above the line of separation.

The theory of the envelope for the line of separation has been under debate for several years. Whether the line of convergence of wall streamlines triggers a vortex flow is of current interest. Perhaps the envelope of converging limiting streamlines truly represents the foot of a separation surface that generates a vortex flow, which alters the pressure field, or, conceivably, it merely is a local phenomenon inside the boundary layer that imposes no significant effect on the pressure field. The uncertainty has resulted in various names for the envelope in the literature. Clearly, there is little consensus among researchers on the criterion of flow separation in three dimensions or on the conditions of the onset of separation.

The calculation methods using three-dimensional boundary-layer equations allow the envelope of converging wall streamlines to be determined; however, the convergence itself does not guarantee the creation of a vortex flow symbolizing the essential features of three-dimensional separation.[4-8] This restriction of the boundary-layer equations can generally be removed using the Navier-Stokes method. The solution of the Navier-Stokes equations not only gives the limiting flow quantities at the wall but also provides information of the overall shear layer, including conditions at the edge of the boundary layer and beyond.

In the present work, the three-dimensional, Reynolds stress averaged Navier-Stokes equations are solved for the flow over an F-14A aircraft wing. An implicit, approximate factorization, finite-difference scheme is employed. The numerical procedure uses the ARC3D code developed by Pulliam and Steger[9,10] with the standard thin-layer approximation for the viscous terms. The code is modified for low-speed flow capability by adding a far-field characteristic-type boundary condition. A zonal approach is taken to calculate effectively the viscous flow near the surface without requiring a large memory. The results represent the early phase of an overall effort to investigate the deck-landing aerodynamics in an aircraft/ship interface environment. High lift conditions are generated by imposing high angles of attack rather than by treating the flap-down wing configuration. Although the low-speed range is of primary concern in the present research, the high subsonic flight condition is also considered to assess the effect of the freestream Mach number.

Computational Method

The basic computational tool is taken from the transonic Navier-Stokes (TNS) computer code developed by Flores and Holst[11] at NASA Ames Research Center. The TNS code consists of the flow solver (ARC3D) and the multizone grid generation program. Both parts have been modified slightly to meet the objectives of the present work. These modifications are further detailed in the discussion of the overall computational method.

The governing equations, numerical algorithm, and turbulence model used in the TNS computer code have been taken from the Pulliam-Steger ARC3D flow solver.[9,10] This code solves the thin-layer Reynolds stress averaged Navier-Stokes equations. Two numerical algorithms are generally supported by the ARC3D flow solver, including an alternative-direction implicit (ADI) like algorithm of Beam and Warming[12] that solves block-tridiagonal matrices along each coordinate direction and a diagonalized ADI-like algorithm of Pulliam and Chaussee[13] that solves scalar pentadiagonal matrices along each coordinate direction. Both algorithms use standard second-order-accurate central differencing of the governing equations to construct the appropriate spatial differencing technique and artificial dissipation schemes to stabilize the time-integration process.

Basic Equations

The three-dimensional Navier-Stokes equations for a perfect gas in generalized curvilinear coordinates (τ,ξ,η,ζ) can be written in nondimensional form as

$$\frac{\partial}{\partial\tau}\hat{Q}+\frac{\partial}{\partial\xi}(\hat{E}-\hat{E}_v)+\frac{\partial}{\partial\eta}(\hat{F}-\hat{F}_v)+\frac{\partial}{\partial\zeta}(\hat{G}-\hat{G}_v)=0 \quad (1)$$

Presented as Paper 90-0596 at the AIAA 28th Aerospace Sciences Meeting, Reno, NV, Jan. 8-11, 1990; received Feb. 6, 1990; revision received Nov. 8, 1990; accepted for publication Dec. 1, 1990.

*Senior Research Scientist, Systems Department. Associate Fellow AIAA.

where $\hat{Q}$ is the vector of dependent flow variables; $\hat{E}$, $\hat{F}$, and $\hat{G}$ are the inviscid flux vectors; and $\hat{E}_v$, $\hat{F}_v$, and $\hat{G}_v$ are the viscous flux terms. Details of these variables are given in Refs. 10 and 11.

In high Reynolds number flows, the viscous effects are confined to a thin layer near the body surface; for many Navier-Stokes computations, the viscous derivatives along the body are dropped if the governing equations are cast in body-oriented coordinates. Such is the present case where the body surface is mapped onto a constant ζ surface. With this assumption, Eq. (1) simplifies to

$$\frac{\partial}{\partial \tau}\hat{Q} + \frac{\partial}{\partial \xi}\hat{E} + \frac{\partial}{\partial \eta}\hat{F} + \frac{\partial}{\partial \zeta}\hat{G} = Re^{-1}\frac{\partial}{\partial \zeta}S \qquad (2)$$

where only the viscous derivatives in the ζ direction are retained. The expression for $\hat{S}$ is also found in Refs. 10 and 11. The coefficients of viscosity and thermal conductivity for the term S are specified from auxiliary relations. For the range of Reynolds numbers of interest in the present work, the flow is turbulent and the two-layer eddy-viscosity model of Baldwin and Lomax[14] is used. The Baldwin-Lomax model is known to be computationally efficient and reasonably accurate for most attached turbulent flow applications. The accuracy starts to deteriorate when the flow separates. Satisfactory results have been obtained in many previous applications, including flows with mild flow separation.

An implicit, approximate factorization of the Beam-Warming-type finite-difference scheme is employed. The basic Beam-Warming algorithm is first- or second-order accurate in time and second-order accurate in space. The equations are factored (spatially split) for a given time step, which reduces the iteration process to three one-dimensional problems. Because of the second-order central-difference operators employed, the algorithm produces block-tridiagonal systems for each spatial dimension.[11]

The finite-difference algorithm of Beam and Warming[12] applied to Eq. (2) results in an approximate factorization. The algorithm produces block-tridiagonal matrices, and the matrix inversion takes extensive computational time. To overcome this difficulty, the ARC3D program also uses the diagonal version of the standard algorithm of Pulliam and Chaussee.[13] In this algorithm, rather than inverting block-tridiagonal matrices in each direction, scalar pentadiagonal matrices are inverted. This computational procedure is more efficient in two ways: 1) the matrix inversions are much simpler, and 2) the fourth-order-implicit artificial dissipation can be added easily to the algorithm. This allows larger time steps and, therefore, faster convergence.

The TNS code and its flow solver ARC3D code have been developed primarily for transonic and/or supersonic flow computations. For these speed ranges, the addition of artificial dissipation models plays an important role in maintaining the numerical stability and controlling strong nonlinear effects such as shocks. In low-speed applications, however, the convergence of the solution is slow and relatively insensitive to the value of the dissipation added.

Zonal Grid

To effectively calculate the viscous flow near the surface without requiring a large memory, the zonal grid approach is adapted. The basic work uses the patched grid zoning method in a grid-refinement mode. A coarse block (grid 1) is first generated about the wing configuration using the parabolic solver approach of Edwards.[15] This single-zone base grid, having an H-mesh topology in both the spanwise and chordwise directions, includes the entire flowfield and contains no viscous clustering. The outermost freestream boundaries are set at four chord lengths away for both upper and lower flowfields. The geometry solution of the Edwards code is modified to handle arbitrary wing geometry including sweeping and dihedral effects. The present version of the code allows direct reading of the coordinates that define the wing geometry.

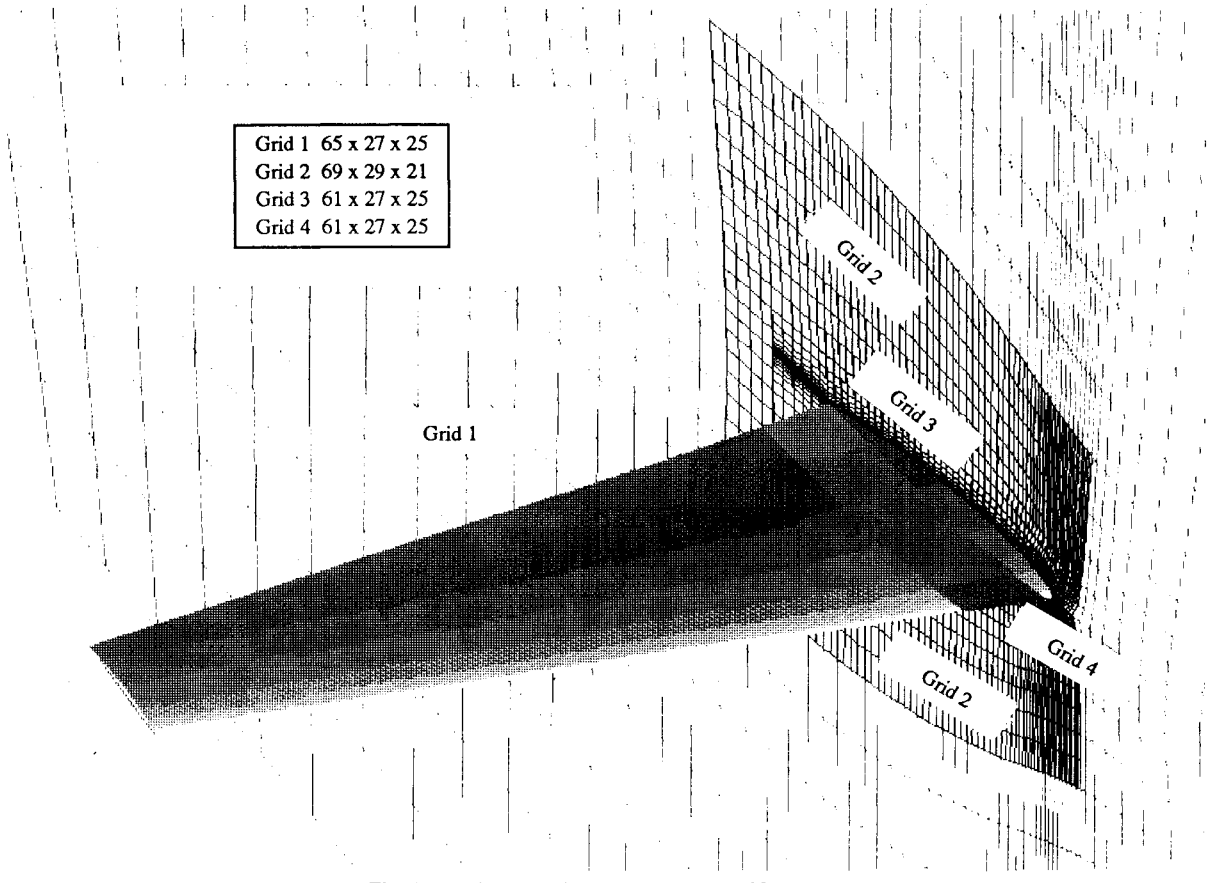

Fig. 1 F-14A aircraft wing and zonal grid.

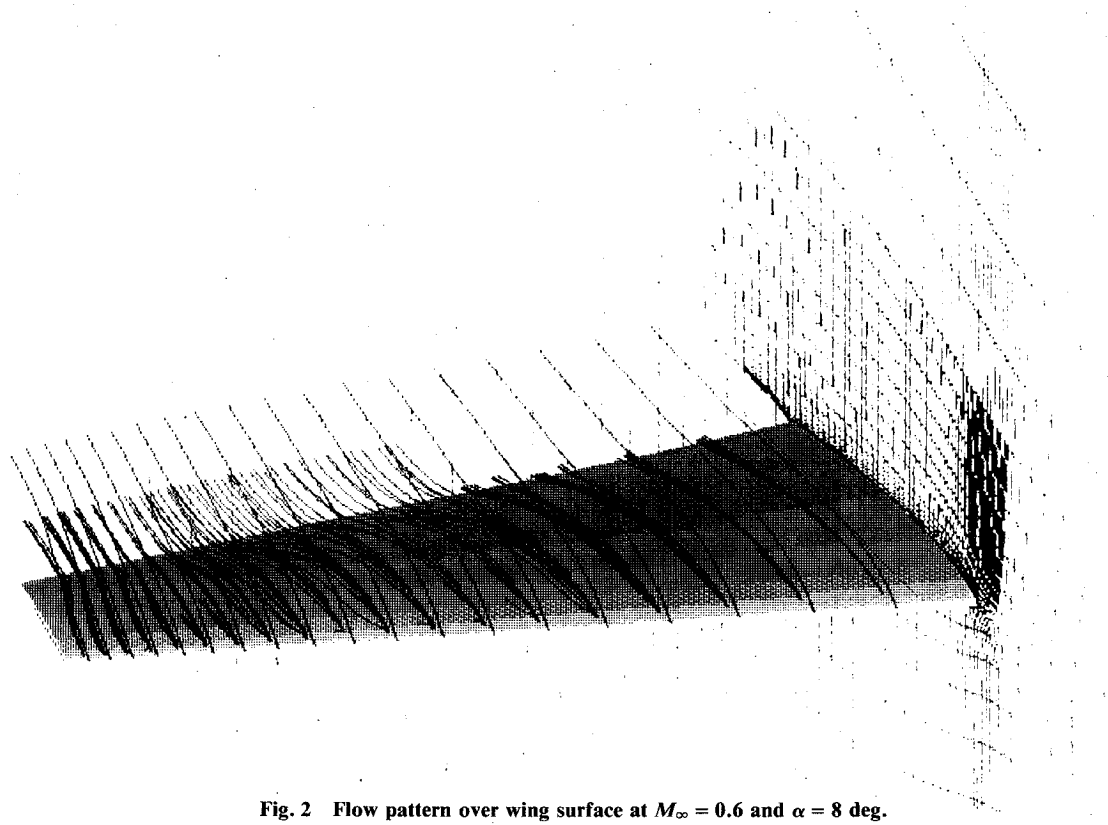

Fig. 2 Flow pattern over wing surface at $M_\infty = 0.6$ and $\alpha = 8$ deg.

Once the base grid is generated, a zoning algorithm is used to divide the grid into separate zones. The first grid zone (grid 1) is the base grid itself with a small block of grid points near the wing removed. The second grid zone (grid 2) basically occupies the space left open by the block of points removed from grid 1 with a small region of overlap included (usually one or two grid cells on all boundaries). Grid 2 is constructed so as to contain twice as many grid points in each spatial direction of the original base grid. This refinement of grid 2 relative to the base grid is accomplished via cubic-spline interpolation. By the same token, the viscous grids (grids 3 and 4) are generated in the vicinity of the upper and lower surfaces within grid 2. These grids are constructed so as to contain the same number of points in both the spanwise and chordwise directions as grid 2. However, the grid points in the normal direction are highly clustered to capture viscous effects on the wing surfaces. Grid 3 is designed to capture the upper wing surface viscous effects and grid 4 to capture the lower wing surface viscous effects. The two outer inviscid grid zones are topologically represented in the computational domain as cubes with smaller cubes removed from the middle. The third and fourth viscous zones are topologically represented as simple cubes in the computational domain.

Figure 1 shows the wing configuration and its four-zone grids in a perspective view. The total number of grid points used in the grid of Fig. 1 is 168,246. The individual grid point breakdown for each zone is the following: grid 1, $65 \times 27 \times 25$; grid 2, $69 \times 29 \times 21$; grid 3, $61 \times 27 \times 25$; and grid 4, $61 \times 27 \times 25$.

Communication between the blocks is achieved via an interpolation procedure. The grid zones are carefully (but automatically) constructed to overlap by two cells. Then, information required at the boundary of one zone is interpolated from the interior of another zone. The most complicated zonal interface boundary condition involves only a series of linear interpolations.

The interface scheme is organized such that only the two planes involved in the interpolation need be defined: base and target planes. These interface surfaces, referred to as planes in the computational domain, are actually curved three-dimensional surfaces in the physical domain. Each boundary plane at a grid zone interface, which requires data for boundary conditions, is called a target plane; each interior plane, which supplies interpolated data to a target plane, is called a base plane. These target and base planes are grouped into three categories: J planes, K planes, and L planes. Each is defined by six integers. For example, the J planes are defined by 1) the grid zone number, 2) the J plane number, 3) the starting K index, 4) the ending K index, 5) the starting L index, and 6) the ending L index. The K and L planes are defined in a similar way.

Although straightforward, the procedure is tedious and involves some data management process if the code is run in a computer with external storage capacity such as the Cray-XMP/YMP. More details are given in Flores and Holst.[11]

Boundary Conditions

The boundary condition treatment of the TNS code applies in the present F-14A wing case, except that the inflow and outflow boundaries are treated differently. Basically, at the far-field (outermost and side, grid 1) boundaries, freestream values are specified; at the solid surfaces (grids 3 and 4), the no-slip condition applies for the three velocity components.

To enhance the convergence of the solution for low-speed flows, the characteristic-like far-field boundary conditions are employed in grid 1. Suggested by Pulliam,[16] the $\hat{Q}$ values at the inflow and outflow boundaries are updated by specifying and extrapolating proper flow variables similar to Rai.[17] Since grid 1 is of H type, the left boundary is the inflow plane and the right boundary is the outflow plane. At the left boundary, four quantities must be specified: a Riemann invariant R_1, the entropy S, and the radial and tangential velocity components, that is,

$$R_1 = u + \frac{2a}{\gamma - 1} \tag{3}$$

$$S = \frac{p}{\rho^\gamma} \tag{4}$$

$$v = 0 \tag{5}$$

$$w = 0 \tag{6}$$

The fifth quantity, another Riemann invariant R_2, is extrapolated from the interior of grid 1:

$$R_2 = u - \frac{2a}{\gamma - 1} \tag{7}$$

This completes the set of five conditions required for five unknowns. At the outflow boundary, there is only one incoming characteristic, hence, only one quantity has to be specified, i.e., the Riemann invariant R_1 is set to its freestream value. The three velocity components along with the entropy are extrapolated from inside.

The implementation of the characteristic-like boundary condition significantly accelerates the convergence of the solution for low-speed flows. Previous application of the concept to transonic flow yields dramatic improvement to the accuracy of the solution.[11] In both cases, the central idea is to satisfy the freestream condition consistently at the far-field boundary, which is rather sensitive for flow computations in these speed ranges.

The whole code has also been converted for Cray-2 operation by eliminating all data management schemes employed in the original TNS code. To distinguish the new features of the code, the new version is designated as the TNSN code. The Ames PLOT3D program[18] has been used extensively in the postprocessing of the numerical results.

Results and Discussion

Numerical results are obtained for an F-14A aircraft wing with a sweep angle of 20 deg traveling at an altitude of 45,000 ft above sea level at $M_\infty = 0.6$ and at sea level at $M_\infty = 0.1$. These conditions, which represent the fighter's normal operation range, yield a Reynolds number of 8.95×10^6. The angle of attack varies from 0 to 12 deg with a 4-deg interval. For the case of Mach 0.6, however, the maximum angle of attack for a converged solution is 10 deg. The flow is turbulent, and the Baldwin-Lomax turbulence model is applied. Results are presented in the form of particle traces, pressure distribution, and lift and drag coefficients. A typical run requires 1100–1500 iterations for a converged solution and takes about 1.5–2.0 h of CPU time on a Cray-2 computer.

Figures 2–4 show the particle traces of viscous and inviscid streamlines emanating from various stations on the upper wing surface for the wing at $M_\infty = 0.6$ at $\alpha = 8$, 9, and 10 deg, respectively. The inviscid streamlines are distinguishable from the viscous streamlines by their position and placidness. In producing these figures, particles are released at four normal locations inside the viscous grid (grid 3) from one level just above the surface to the middle of the viscous grid. Since the particles are allowed to travel through the whole flowfield, the trace should reveal an overall shear-layer phenomenon. At $\alpha = 8$ deg, the viscous streamlines start to converge near the trailing edge (see Fig. 2). As the angle of attack increases to 9 deg, the convergence of the viscous streamlines in the rear region is completed and an envelope is formed along the outer half of the wing (see Fig. 3). The flow essentially is attached, however, since the viscous streamlines are practically confined to the immediate layer above the surface. It is important to recognize that the confinement is unforced; thus, the flow is truly attached regardless of the formation of an envelope, which symbolizes flow separation in a traditional sense.

Flow separation is imminent at this point, however. A further increase of 1 deg in angle of attack triggers massive separation over the entire surface of the wing, as shown in Fig. 4. The massive separation is believed to be caused by the convergence of viscous streamlines represented by the envelope shown in Fig. 3. It is unlikely that the separation may have been triggered by the shock-wave/boundary-layer interaction since the flow remains subcritical over most part of the wing surface. The flow becomes supercritical in only a small area of the leading-edge region near the root—the so-called peaky distribution for typical conventional airfoil/wing sections at high subsonic freestream and angle of attack. The F-14A sections are very similar to those of the conventional

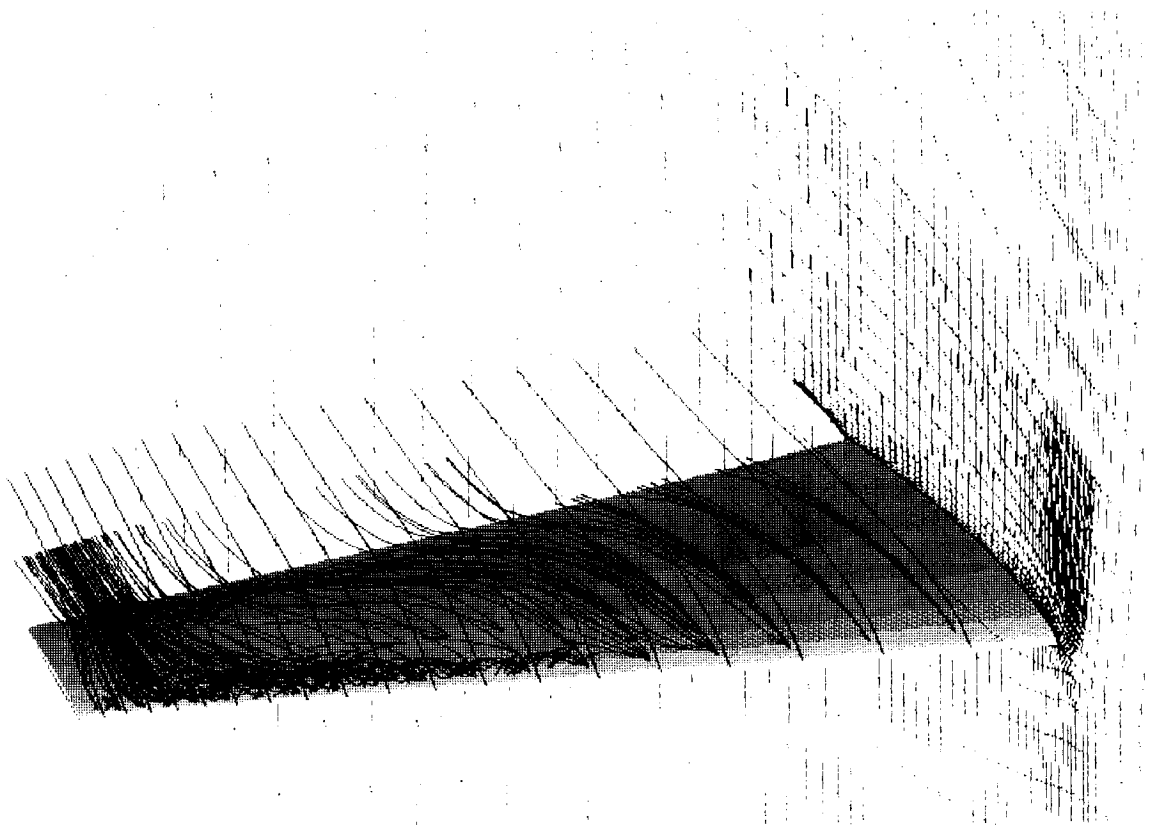

Fig. 3 Flow pattern over wing surface at $M_\infty = 0.6$ and $\alpha = 9$ deg.

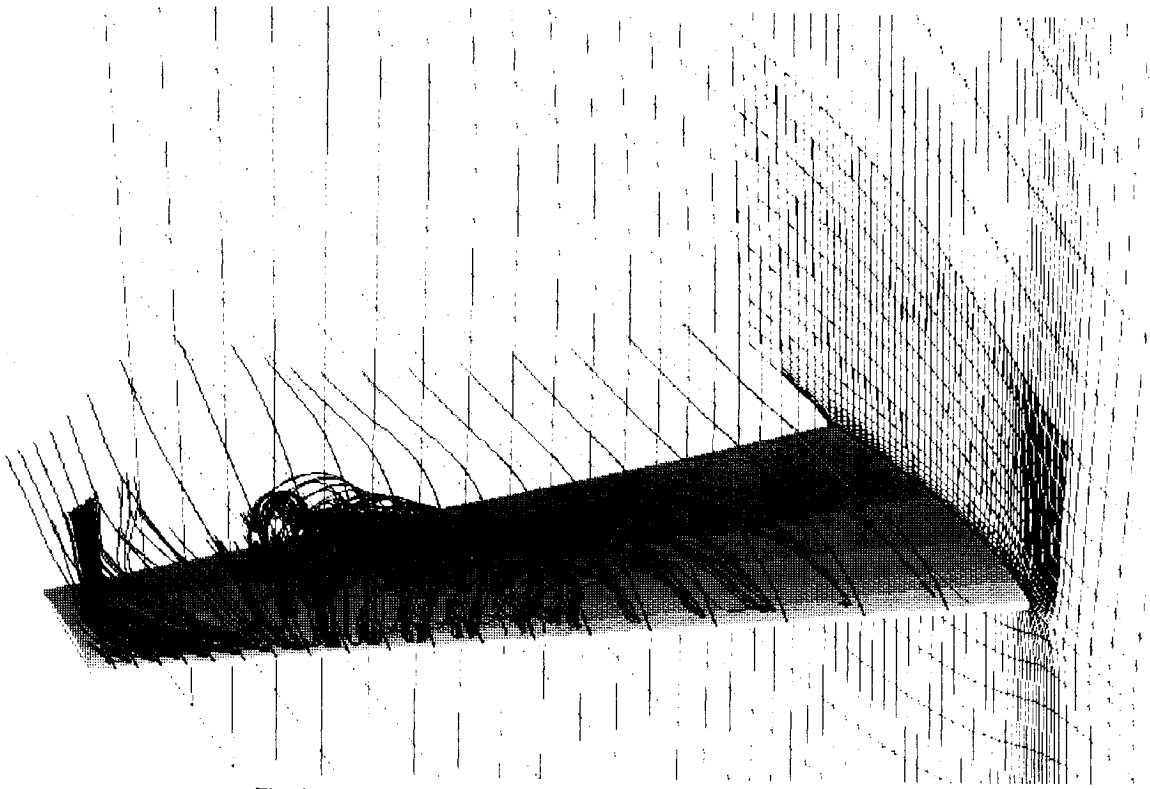

Fig. 4 Flow pattern over wing surface at $M_\infty = 0.6$ and $\alpha = 10$ deg.

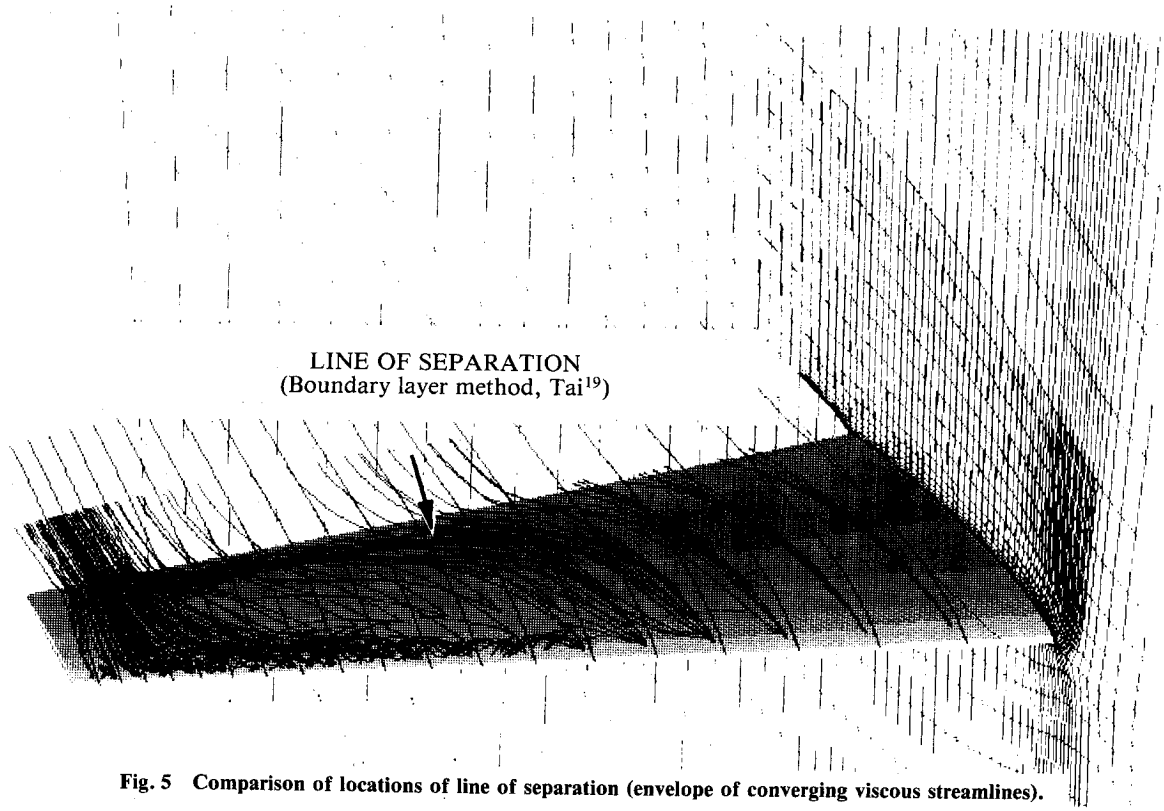

Fig. 5 Comparison of locations of line of separation (envelope of converging viscous streamlines).

NACA-64A410 airfoil. Thus, the appearance of the peaky-type flow is of no surprise.

The anticipated line of separation (the envelope of converging limiting streamlines) and the viscous streamline pattern, for the most part, resemble those obtained earlier using the integral boundary-layer approach.[19] In this approach, which considers only the pure viscous separation (that is, no shock wave at all), the line of separation is detected at $\alpha = 8$ deg. Comparison of the location of separation line is shown in Fig. 5. The slight delay in separation in the present results is believed to be due to the Baldwin-Lomax turbulence model used in the TNSN code. At this point, it is reasonable to assess that the Navier-Stokes method offers much more insight into the flow physics than is possible with the boundary-layer approach. The boundary-layer method is very much limited to the attached flow—at most, the approach is valid up to the formation of the envelope of converging viscous streamlines (line of separation). (The inverse mode of the boundary-layer method has overcome the difficulty due to separation and can be used for small confined separated regions.[8,20])

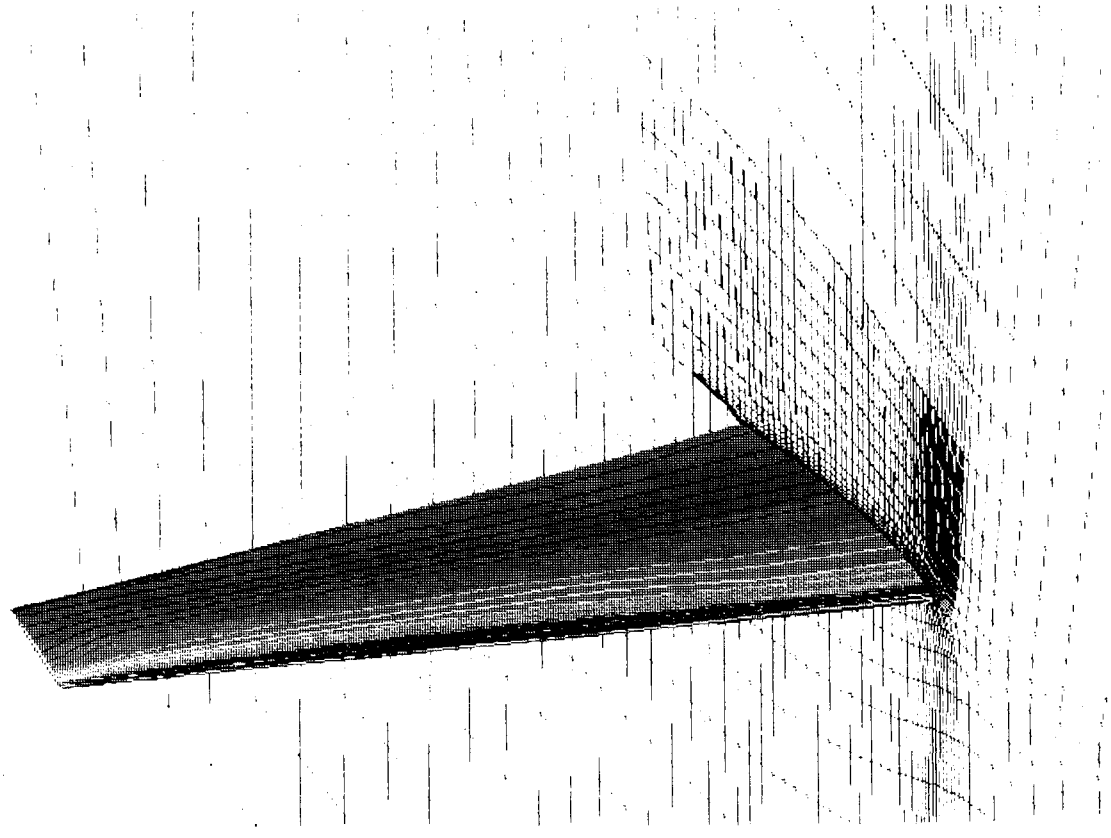

Fig. 6 Pressure coefficient contour for $M_\infty = 0.6$ and $\alpha = 8$ deg.

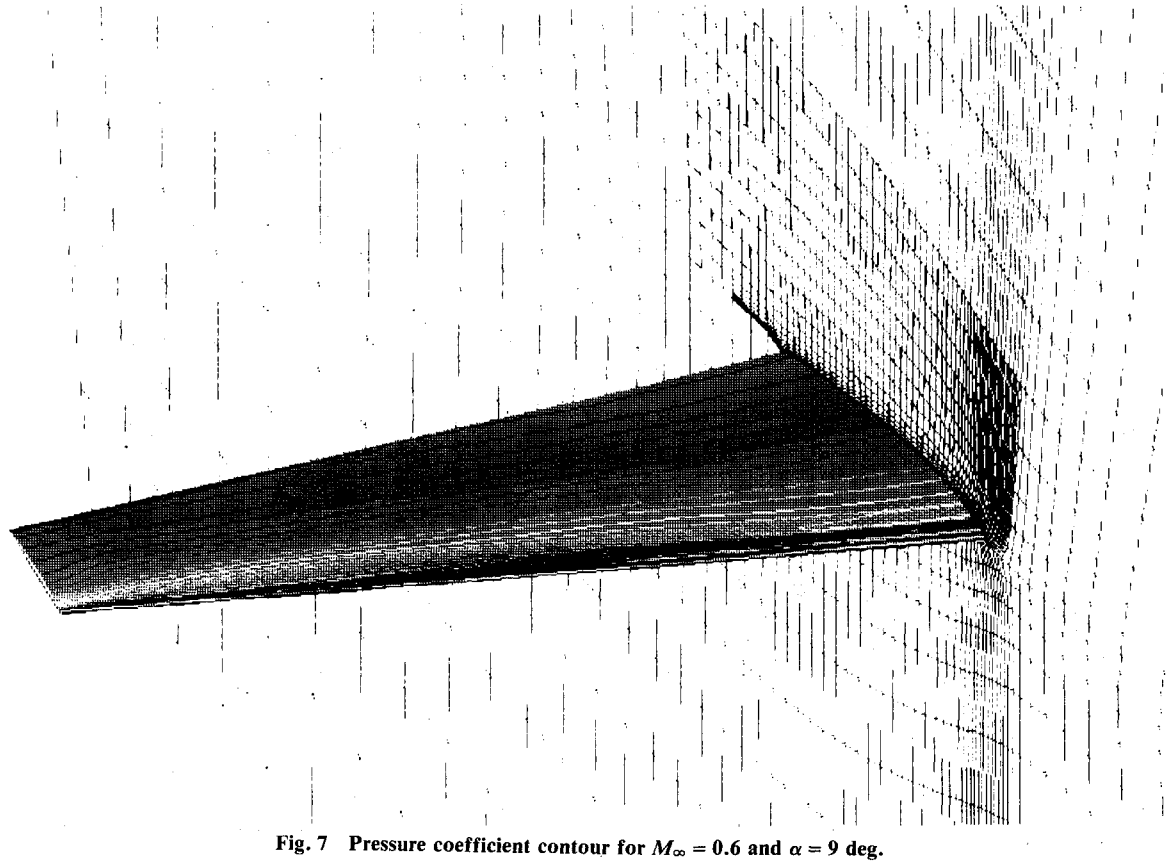

Fig. 7 Pressure coefficient contour for $M_\infty = 0.6$ and $\alpha = 9$ deg.

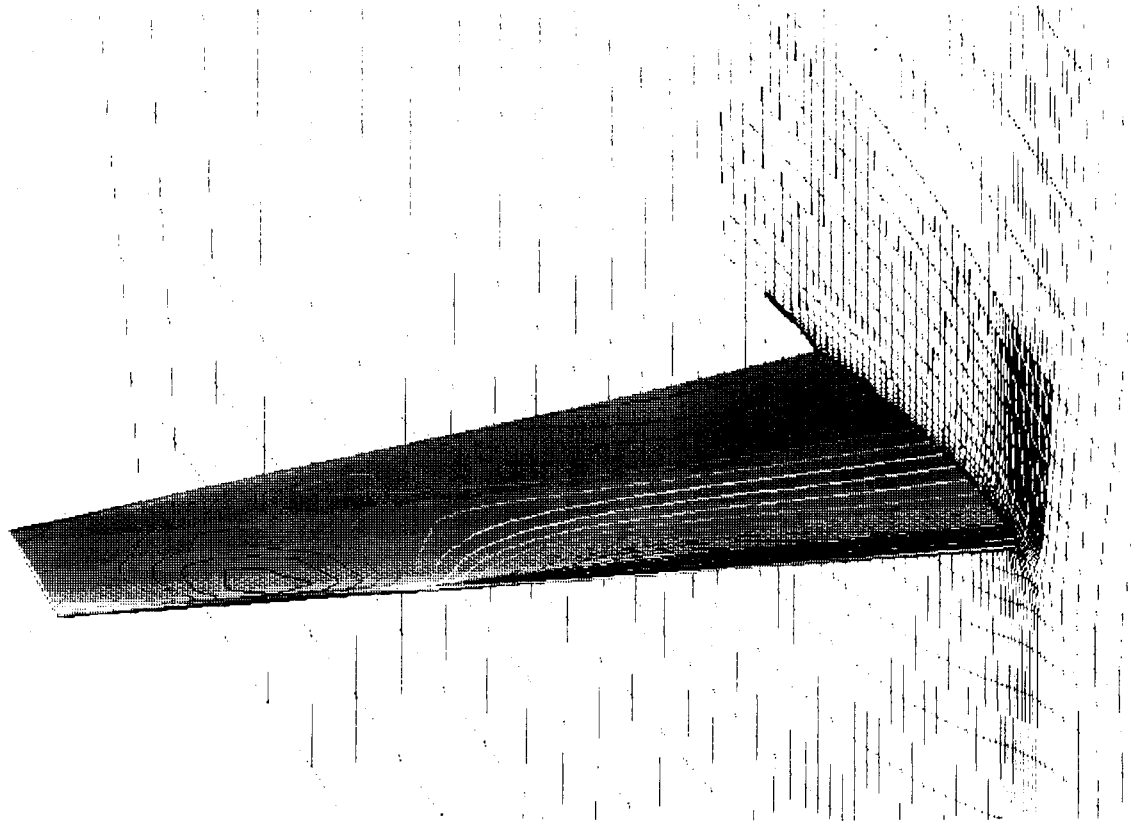

Fig. 8 Pressure coefficient contour for $M_\infty = 0.6$ and $\alpha = 10$ deg.

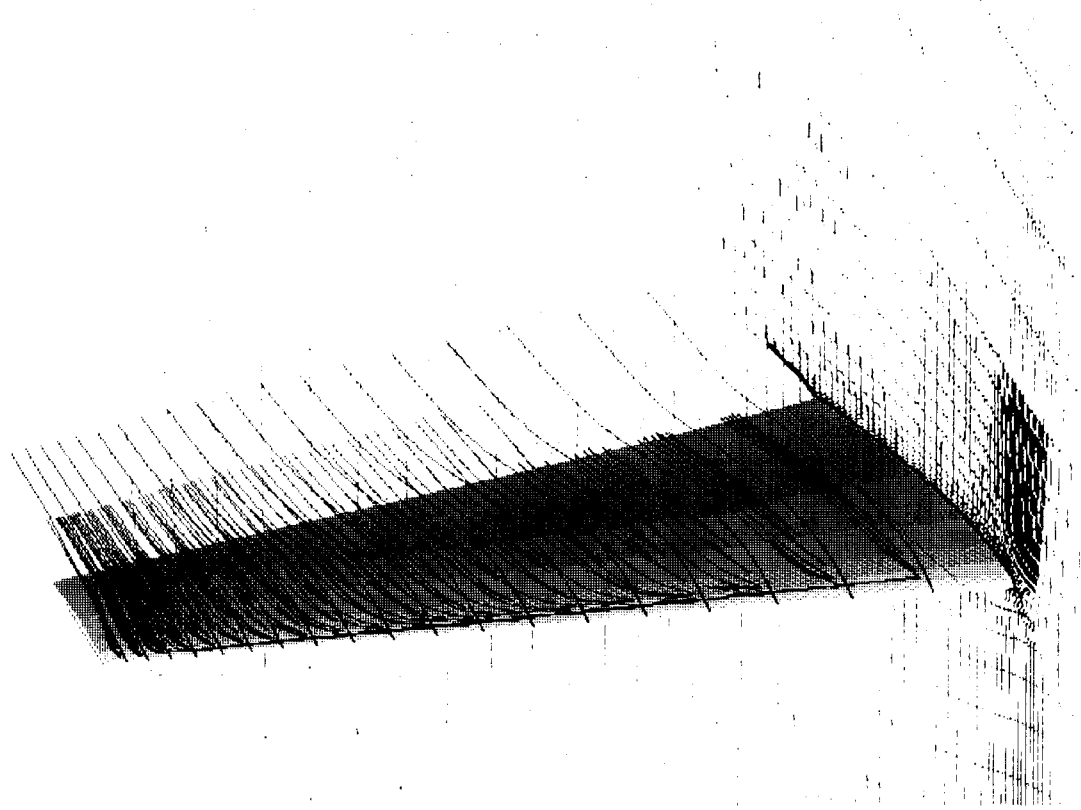

Fig. 9 Flow pattern over wing surface at $M_\infty = 0.1$ and $\alpha = 8$ deg.

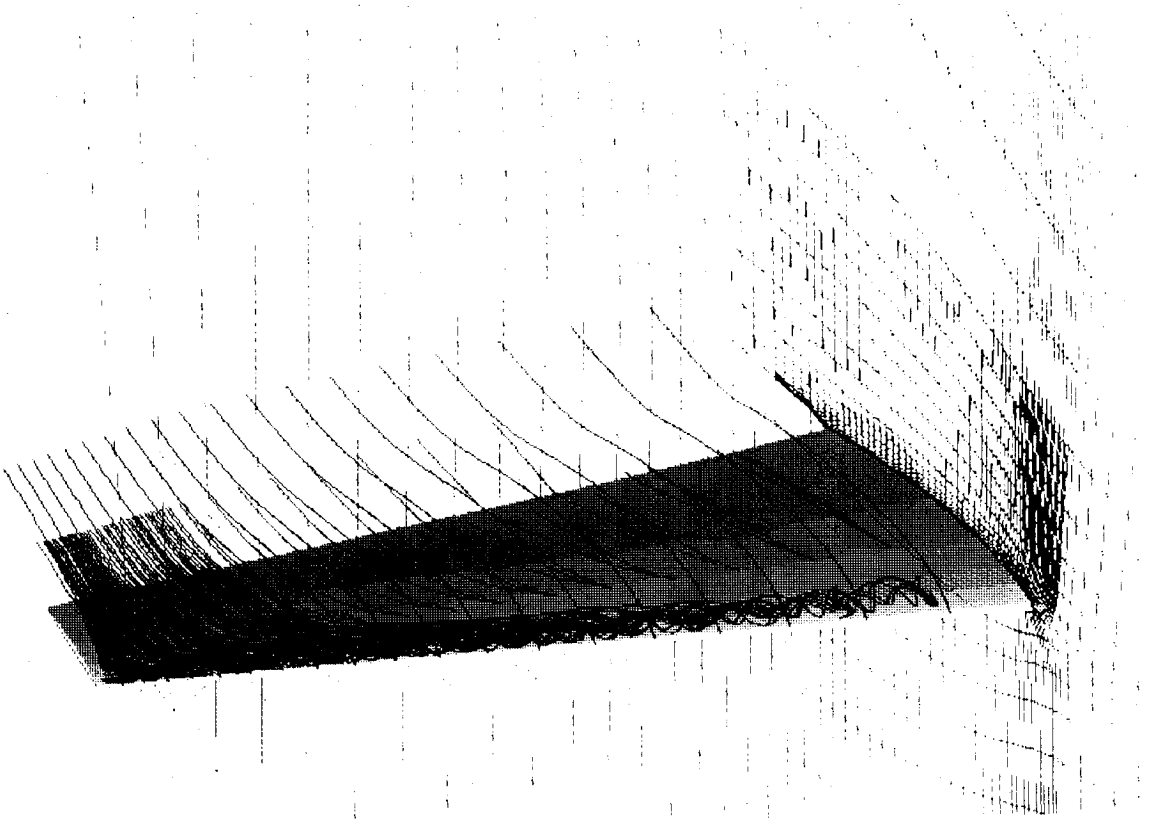

Fig. 10 Flow pattern over wing surface at $M_\infty = 0.1$ and $\alpha = 12$ deg.

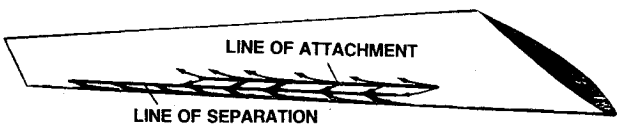

Fig. 11 Schematic of line of separation and line of attachment at $M_\infty = 0.1$ and $\alpha = 8$ deg.

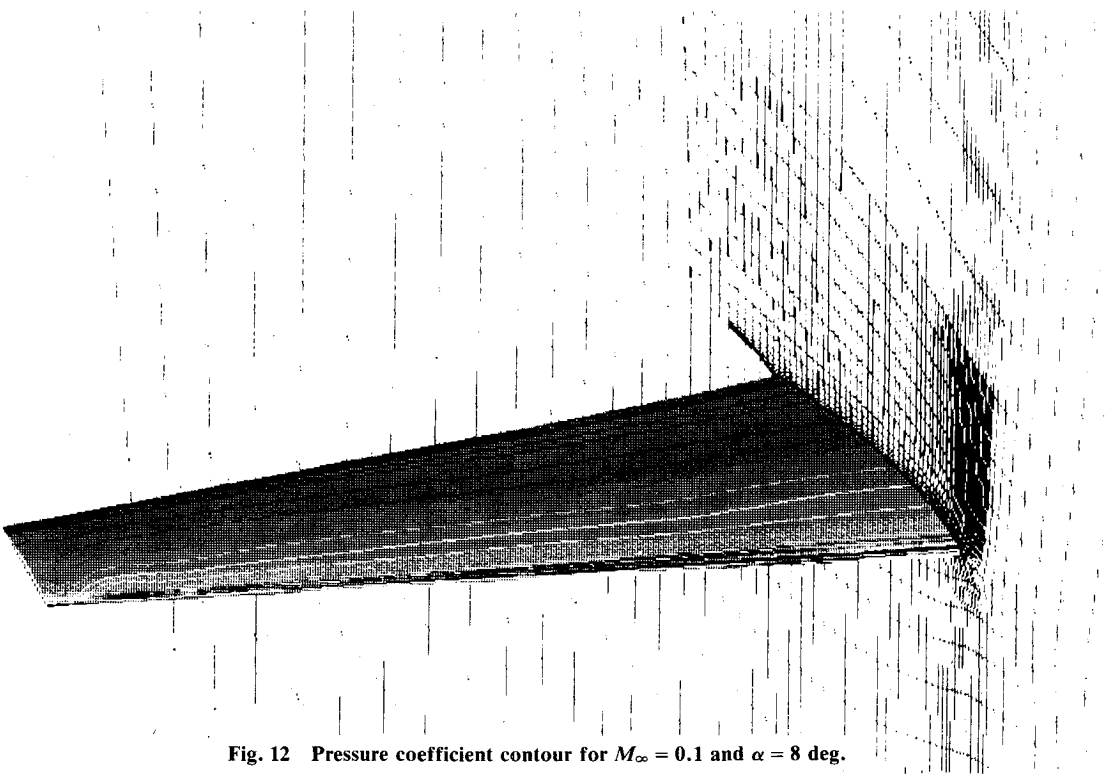

Fig. 12 Pressure coefficient contour for $M_\infty = 0.1$ and $\alpha = 8$ deg.

The appearance of the peaky-type flow is supported by the pressure distribution over the wing shown in Figs. 6–8, corresponding to $\alpha = 8$, 9, and 10 deg, respectively. In general, the pressure contours are fairly orderly in the cases of $\alpha = 8$ and 9 deg, indicating that the flow is essentially attached. Peaky pressures appear in the leading-edge region. For the case of $\alpha = 10$ deg, a drastic change in the pressure pattern is observed, with a large positive pressure region in the outer part of the wing resulting from massive separation.

Of some surprise, however, is the separation pattern that changes when the freestream Mach number reduces to 0.1, which corresponds to a landing situation. At this low speed, but with the same Reynolds number, the rear region massive separation disappears. Instead, a strong leading-edge separation is emerged (see Figs. 9 and 10).

The formation of the leading-edge separation bubble seems to be caused by the high leading-edge vacuum in a moderate pressure gradient environment. It is observed that at $\alpha = 8$ deg

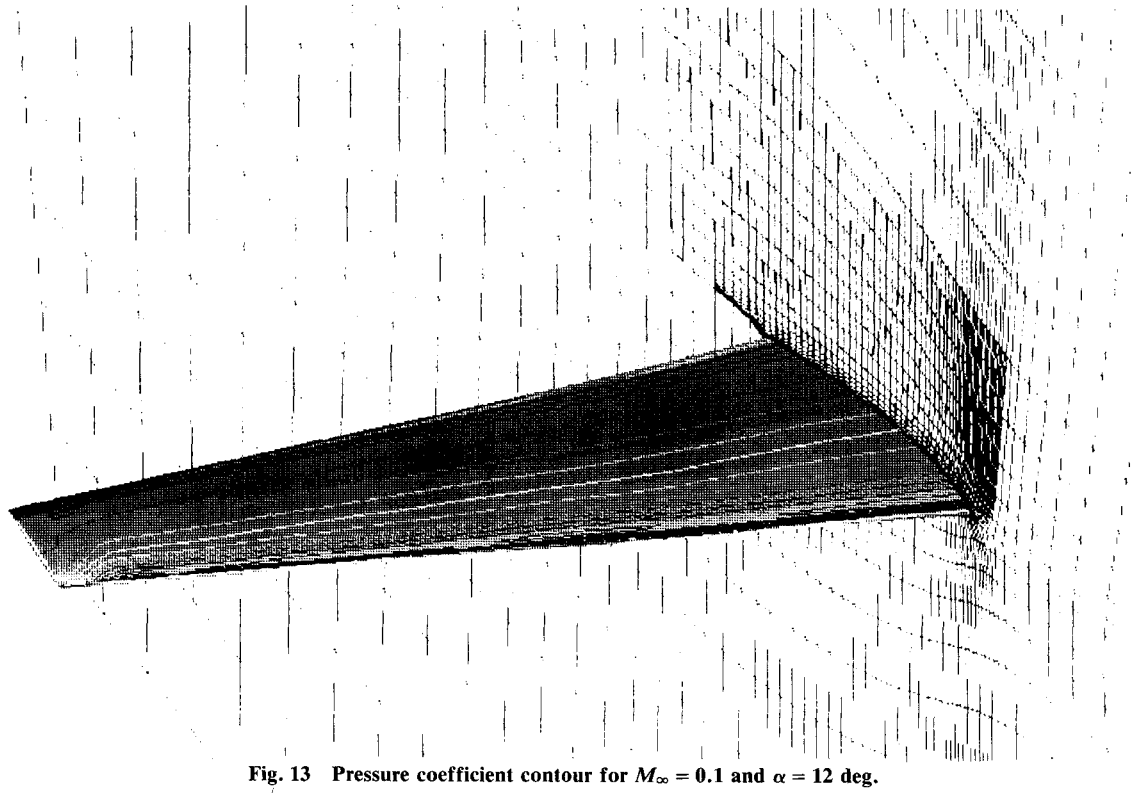

Fig. 13 Pressure coefficient contour for $M_\infty = 0.1$ and $\alpha = 12$ deg.

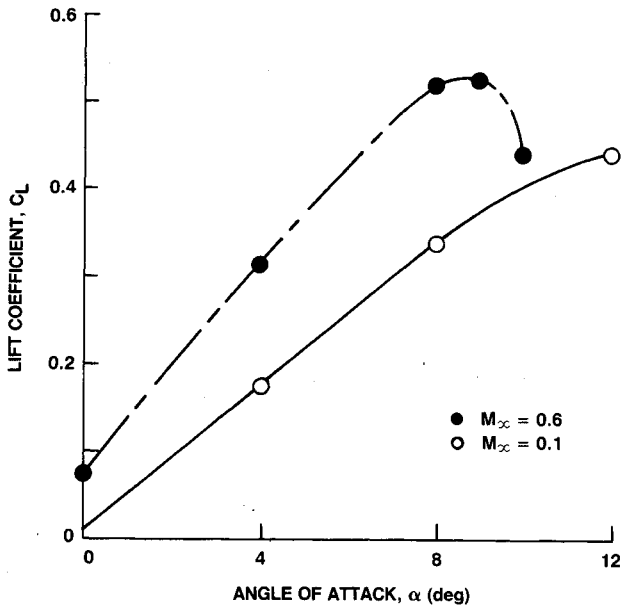

Fig. 14 Lift coefficient vs angle of attack.

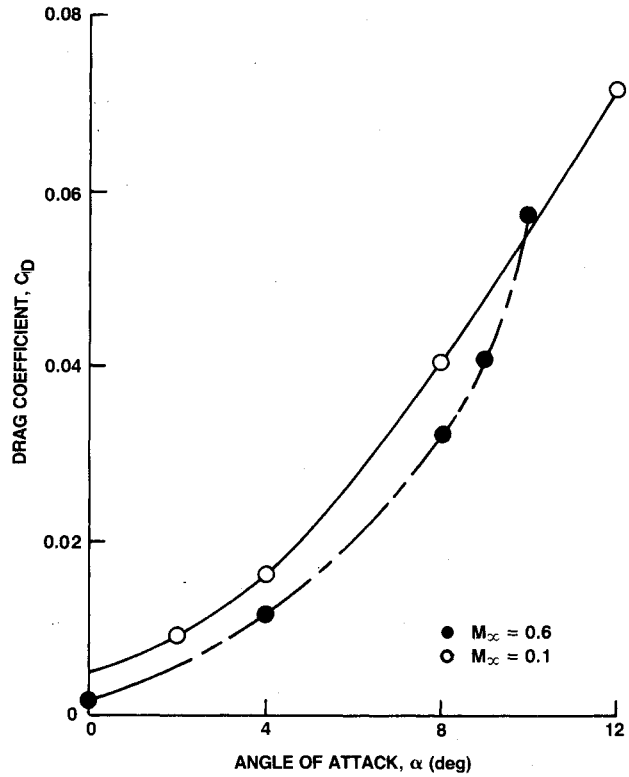

Fig. 15 Drag coefficient vs angle of attack.

($M_\infty = 0.1$) there is convergence of viscous streamlines in the leading-edge region. Particles adjacent to the surface released from the first two chordwise locations start to converge and result in a separation line at about one-third span of the wing (see Fig. 11). At the same angle of attack, but at high speed ($M_\infty = 0.6$, Fig. 3), such a convergence is almost not noticeable. (Convergence of leading-edge limiting streamlines at high speed starts at $\alpha = 9$ deg but appears to be less dominant than that in the rear region.) As the angle of attack increases, the convergence becomes more apparent. Finally, at $\alpha = 12$ deg, a very strong vortex separation bubble is formed (see Fig. 10).

Theoretically, all surface streamlines are driven by the pressure gradients, shear stress gradients, and geometric constraints.[4] The effects of these factors are global and cumulative. The power of the Navier-Stokes code combined with the PLOT3D routine allows complete exhibition of these theoretical aspects. In other words, it is now possible to detect the detailed flow features laid down by the theory some time ago. What really occurs here is a line of attachment (divergence of viscous streamlines) immediately aft of the leading-edge separation bubble, as shown in Fig. 11. It is from this line of attachment that the viscous streamlines emanate in both upstream and downstream directions. Those toward upstream converge to the line of separation that provides the footing of the leading-edge separation bubble. Those emanating downstream lead to a flow reattachment after the leading-edge separation bubble. The smooth pressure distribution patterns for those cases (Figs. 12 and 13) imply that the flow is completely attached after the reattachment.

Unlike the effect of Reynolds number, the effect of Mach number (with fixed Reynolds number) on three-dimensional flow separation is less known and seldom investigated. The present results reveal that the redistribution of surface pressures due to the change of freestream Mach number in fact changes the resulting flow pattern. In three-dimensional flows, the outer surface pressure influences the boundary-layer behavior in two ways: 1) the boundary layer being acted upon by the pressure distribution, i.e., the usual boundary-layer development; and 2) the viscous streamlines inside the boundary layer being acted upon by the external streamline pattern, which is dictated by the pressure gradients. The latter is intrinsic to three-dimensional flows and becomes more dominant when the vehicle is at a large angle of attack. The increase in freestream Mach number here has certainly changed external streamline pattern, which, in turn, leads to the convergence of viscous streamlines and eventually the flow separation.

Although the lift coefficients (Fig. 14) generally are lower and the drag coefficients (Fig. 15) are higher at low speed, they are far more stable as the angle of attack increases. It is believed that, although the leading-edge separation is fairly strong at low speed, its impact on the surface pressure distribution is light compared to the trailing-edge separation. On the other hand, the rapid increase in the drag values at $M_\infty = 0.6$ at high angles of attack confirms the existence of massive flow separation.

Acknowledgments

This work was supported by the Office of the Chief of Naval Research, the Naval Air Systems Command, and the Independent Research Program at David Taylor Research Center. The supercomputer resources were provided by NASA Ames Research Center. The author wishes to thank J. Flores, T. H. Pulliam, and T. L. Holst of NASA Ames Research Center for their helpful discussions.

References

[1]Eichelbrenner, E. A., and Oudart, A., "Methods de Calcul de la Couche Limite Tridimensionelle. Application a un Corps Fusele Incline sur le Vent," ONERA Pub. 76, Chatillon, France, April 1955.

[2]Maxwell, E. C., "Flow Separation in Three Dimensions," Royal Aircraft Establishment, Rept. Aero 2565, Bedford, England, UK, Nov. 1955.

[3]Wang, K. C., "Separation Patterns of Boundary Layers over an Inclined Body of Revolution," *AIAA Journal,* Vol. 10, No. 8, 1972, pp. 1044–1050.

[4]Tai, T. C., "Determination of Three-Dimensional Flow Separation by a Streamline Method," *AIAA Journal,* Vol. 19, No. 10, 1981, pp. 1264–1271.

[5]Tai, T. C., "Application of Two-Dimensional Velocity Profile to Three-Dimensional Boundary-Layer Flow," *AIAA Journal,* Vol. 24, No. 3, 1986, pp. 370–377.

[6]Ragab, S. A., "Steady and Unsteady Boundary Layers on Prolate Spheroids at High Incidence," AIAA Paper 85-1708, July 1985.

[7]Van Calsem, W. R., and Steger, J. L., "The Efficient Simulation of Separated Three-Dimensional Viscous Flows Using the Boundary Layer Equations," AIAA Paper 85-4064, Oct. 1985.

[8]Radwan, S. F., and Lekoudis, S. C., "Inverse Mode Calculations of the Incompressible Turbulent Boundary Layer on an Ellipsoid," *AIAA Journal,* Vol. 24, No. 10, 1986, pp. 1628–1635.

[9]Pulliam, T. H., and Steger, J. L., "Implicit Finite-Difference Simulations of Three-Dimensional Compressible Flow," *AIAA Journal,* Vol. 18, No. 2, 1980, pp. 159–167.

[10]Pulliam, T. H., "Euler and Thin Layer Navier-Stokes Codes: ARC2D, ARC3D," Notes for Computational Fluid Dynamics User's Workshop, Univ. of Tennessee Space Inst., Tullahoma, TN, March 1984.

[11]Flores, J., and Holst, T. L., "Numerical Solution of the Navier-Stokes Equations for Complex Configurations," Lecture Series in Computational Fluid Dynamics, Univ. of Tennessee Space Inst., Tullahoma, TN, March 1988,

[12]Beam, R., and Warming, R. F., "An Implicit Finite-Difference Algorithm for Hyperbolic Systems in Conservation-Law Form," *Journal of Computational Physics,* Vol. 22, Sept. 1976, pp. 87–110.

[13]Pulliam, T. H., and Chaussee, D. S., "A Diagonal Form of an Implicit Approximate-Factorization Algorithm," *Journal of Computational Physics,* Vol. 39, No. 2, 1981, pp. 347–363.

[14]Baldwin, B. S., and Lomax, H., "Thin-Layer Approximation and Algebraic Model for Separated Turbulent Flows," AIAA Paper 78-257, Jan. 1978.

[15]Edwards, T. A., "Noniterative Three-Dimensional Grid Generation Using Parabolic Partial Differential Equations," AIAA Paper 85-0485, Jan. 1985.

[16]Pulliam, T. H., private communication, April 1988.

[17]Rai, M. M., "Unsteady Three-Dimensional Navier-Stokes Simulations of Turbine Rotor-Stator Interaction," AIAA Paper 87-2058, June 1987.

[18]Walatka, P. O., and Buning, P. G., "PLOT3D User's Manual," NASA TM-101067, Jan. 1990.

[19]Tai, T. C., "An Integral Method for Three-Dimensional Turbulent Boundary Layer with Large Crossflow," AIAA Paper 87-1254, June 1987.

[20]Carter, J. E., "A New Boundary-Layer Inviscid Iteration Technique for Separated Flow," AIAA Paper 79-1450, July 1979.